

D. G. Liebermann · A. Biess · C. C. A. M. Gielen
T. Flash

Intrinsic joint kinematic planning. II: Hand-path predictions based on a Listing's plane constraint

Received: 24 October 2004 / Accepted: 5 September 2005 / Published online: 8 December 2005
© Springer-Verlag 2005

Abstract This study was aimed at examining the assumption that three-dimensional (3D) hand movements follow specific paths that are dictated by the operation of a Listing's law constraint at the intrinsic joint level of the arm. A kinematic model was used to simulate hand paths during 3D point-to-point movements. The model was based on the assumption that the shoulder obeys a 2D Listing's constraint and that rotations are about fixed single-axes. The elbow rotations were assumed to relate linearly to those of the shoulder. Both joints were assumed to rotate without reversals, and to start and end rotating simultaneously with zero initial and final velocities. Model predictions were compared to experimental observations made on four right-handed individuals that moved toward virtual objects in "extended arm", "radial", and "frontal plane" movement types. The results showed that the model was partially successful in accounting for the observed behavior. Best hand-path predictions were obtained for extended arm movements followed by radial ones. Frontal plane movements resulted in the largest discrepancies between the predicted and the observed paths. During such movements, the upper arm rotation vectors did not obey Listing's law and this may explain the observed discrepancies. For other movement types, small deviations from the predicted paths were observed which could be explained by the fact that sin-

gle-axis rotations were not followed even though the rotation vectors remained within Listing's plane. Dynamic factors associated with movement execution, which were not taken into account in our purely kinematic approach, could also explain some of these small discrepancies. In conclusion, a kinematic model based on Listing's law can describe an intrinsic joint strategy for the control of arm orientation during pointing and reaching movements, but only in conditions in which the movements closely obey the Listing's plane assumption.

Keywords Listing's law · Joint kinematics · End-point path model

Introduction

The present study investigated the principles underlying the formation of end-point paths during three-dimensional (3D) reaching and pointing movements based on the assumption that hand trajectories are dictated by laws of control imposed on the arm at the joint level.

A substantial number of early studies (Morasso 1981; Abend et al. 1982) have argued in favor of the idea that multi-joint movements are planned in terms of extrinsic hand coordinates. According to these studies, nearly straight hand paths with bell-shaped tangential velocity profiles characterize 2D reaching movements. Flash and Hogan (1985) developed an optimal control model that predicted the kinematic characteristics of such movements, and concluded that the resulting trajectories are an expression of the intent to minimize the hand jerk.

However, many of the hand movement studies that propose planning in terms of extrinsic coordinates have been validated only for relatively simple movements performed in the horizontal plane. Few models have been developed to explain other, more complex, motion patterns like drawing scribbles or handwriting. In an early attempt to describe the planning and control of such curved movement types, Viviani and Terzuolo (1982) suggested the "two-thirds power law". Based on

D. G. Liebermann (✉)
Department of Physical Therapy,
Sackler Faculty of Medicine, Tel-Aviv University,
69978 Ramat Aviv, Israel
E-mail: dlieberm@post.tau.ac.il
Tel.: +972-3-6405589
Fax: +972-3-6405436

A. Biess · T. Flash · D. G. Liebermann
Department of Applied Mathematics and Computer Science,
Weizmann Institute of Science, 76100 Rehovot, Israel

C. C. A. M. Gielen
Department of Medical Physics and Biophysics,
University of Nijmegen, 6525 EZ Nijmegen, The Netherlands

experimental observations, they found that the angular velocity at the end-point (A) decreases as a function of the increases in the curvature of the path (K) following the relationship $A \approx CK^{2/3}$, where C is a piecewise velocity gain factor. C can also be expressed as $1/r$ (the inverse of the radius of the curvature r). This invariant relationship between curvature and velocity may be defined more practically for the end-point tangential velocity (V) as $V \approx CK^{-1/3}$.

In an attempt to unify the minimum jerk and the two-thirds power law, Viviani and Flash (1995) proposed that kinematic planning of curved and straight point-to-point movements obey a common strategy. In both cases, the assumed goal of the performance is to maximize smoothness at the extrinsic hand level. More recently, Richardson and Flash (2002) provided a theoretical basis for the unification of the two theoretical accounts, although it has been argued also that the two-thirds power law is an epiphenomenon of some other principles (Todorov and Jordan 1998) such as being a byproduct of the intent to perform smooth joint trajectories (Schaal and Sternad 2001).

The suggestion that hand movement control may be carried out by intrinsic level planning is not new. Soechting and Lacquaniti (1981) argued that joint kinematic planning is used during planar vertical movements performed in a sagittal plane, and showed experimentally that the shoulder and elbow rotations are linearly related. Atkeson and Hollerbach (1984) confirmed the same linear relationship between joint velocities during similar movements, and proposed a “linear joint interpolation strategy” to account for the experimental observations. According to this strategy, curved hand paths at the extrinsic level are the result of a constant ratio between the angular velocities of the shoulder and elbow joints. Hollerbach and Atkeson (1986) have also noticed that these hand paths become straight toward the boundaries of the workspace, and proposed a “staggered joint interpolation strategy” (Hollerbach and Atkeson 1987) to explain such a phenomenon. Their model allows for the onset and offset of the movement in one joint to be delayed with respect to those of an adjacent joint, and consequently, at the extremes of the workspace the path turns to be straight. Other studies have provided additional support for joint-level planning (Kaminski and Gentile 1986; Flanagan and Ostry 1989). These studies share the assumption that intrinsic joint kinematics capture major characteristics of the trajectory planning process. Evidence showing that intrinsic arm dynamics (and not only intrinsic kinematics) may determine the extrinsic characteristics of the hand trajectories has also been reported from modeling approaches that involve the minimization of the rate of change of joint torques (Uno et al. 1989) and the minimization of the rate of change of the commanded torques (Nakano et al. 1999).

Taken together, these studies advocate that joint-level planning may simplify the computational problems associated with motion planning in terms of end-point

coordinates. Models based on intrinsic joint-level planning are often considered more realistic since the underlying assumptions include the notion that the brain takes into account intrinsic limb properties (not only the geometric characteristics of the end-point path). A major problem common in this approach is the inverse kinematics problem, which does not have a unique solution for a kinematically redundant arm moving in three dimensions. Only few of those models have attempted to explain how the system copes with kinematic redundancies.

An attempt to deal with 3D movements has been made by Soechting and Terzuolo (1988), who assumed that a decrease in movement variability during motor execution is an expression of the level of motion planning that the brain uses in order to generate a movement. Their empirical evidence showed that the arm joint trajectories were less variable than the end-point trajectories during 3D drawing movements, and interpreted their results as evidence in support of a planning scheme at the joint level. Soechting et al. (1995) further developed an intrinsic model based on the minimization of peak kinetic energy during pointing to visual targets with the hand in three dimensions. Their model accounted for the deviations of the arm orientation at the end of the movement from postures predicted by Donders’ law. However, their model did not make any predictions concerning the expected hand paths.

More recently, Biess et al. (2001) went a step further and developed a model that simultaneously predicted arm postures and the corresponding hand paths. Biess et al. (2001) analyzed the geometric predictions of the hand path and the final arm posture using a cost function based on the minimization of the kinetic energy of the whole arm. The solution of the optimization problem corresponded to geodesics in the arm configuration space with respect to a metrics defined by the total kinetic energy. Comparisons between the experimental observations and the model results have suggested that 3D joint postures may be influenced by the inertial properties of the whole arm (Biess et al. 2001). Wang (1998) and Wang and Verriest (1998) presented a model for 3D movements as well, but they used a cost function based on the minimization of joint discomfort.

Finally, Torres and Zipser (2002) showed that 3D hand paths and orientations could be closely predicted by applying a gradient descent technique to a cost function that was based on the distance between a specified target and the current arm configuration in an abstract configuration space. Torres and Zipser (2002) suggested that path planning based on geometric constraints is a step that may precede a temporal stage involving the specification of time-dependent joint kinematic variables (velocities and/or accelerations).

Listing’s law has long been suggested as an intrinsic constraint that may be used during 3D eye movements (Westheimer 1957; Collewyn et al. 1988). Tweed and Vilis (1987, 1990) found support for the validity of Listing’s law and the single-axis rotation hypothesis

from their model predicting eye torsion between saccades. Based on similar principles, Straumann et al. (1991) suggested a model for the upper limb rotations during extended arm pointing movements. Miller et al. (1992) expanded this approach and studied Listing's law during hand reaching movements of different types. Only few attempts have been made to incorporate such constraints on joint rotations with the purpose of predicting the actual hand paths during 3D movements (Gielen et al. 1997).

In this part of the study, we assume the validity of Listing's law at the shoulder joint level based on the evidence reported in the accompanying manuscript. This assumption allows to derive shoulder rotations that follow minimal amplitude paths by constraining the joints to rotate about fixed single-axes (i.e., to follow straight lines in a Listing's plane representation). The elbow rotations are assumed to relate linearly to those dictated by Listing's law at the shoulder and this, in turn, allows for the prediction of the hand paths. This modeling approach is carried out as an attempt to gain additional insights into the rules used by the brain to govern the extrinsic characteristics of 3D motion.

Theoretical model

Model assumptions

The first main assumption of the present model is that rotation vectors of the upper arm during pointing and reaching in three dimensions can be described within a reasonable margin of error by a 2D surface.

We have reported previously (Liebermann et al. 2005, manuscript I) that even for a random mixture of movements the coefficients of curvature and twist (d , e , and f) were relatively low when the rotation vectors were fitted to the equation $r_x = a + br_y + cr_z + dr_y^2 + er_yr_z + fr_y^2$. These scores were often found to be not different from zero. We also reported that the thickness of the manifold representing the upper arm rotations about the shoulder was relatively small. Therefore, as first-order approximations, mean Listing's planes were adopted for each movement type in order to describe the upper arm segment rotations. The rotation vectors were assumed to follow straight lines within the assumed planes (i.e., assumed to be single-axis rotations). We extracted the primary position coordinates from the vectors orthogonal to these planes, and used them as reference vectors for the prediction of the arm rotations based on Listing's law.

Our forward modeling approach considers two limb segments for the prediction of the hand paths during pointing and reaching movements. Listing's law for the shoulder does not specify the movement of the forearm. Therefore, in frontal and radial arm movements an additional assumption made here was that the relationship between the elbow joint rotations (flexion–extension) and the shoulder joint rotations is linear. This has

been supported by experimental observations (Marotta et al. 2003), although it may not hold for movements toward the boundaries of the workspace (Hollerbach and Atkeson 1987).

Further assumptions were made in order to determine objective criteria for the exclusion of some experimental trials:

1. The model assumed that hand movements toward visual targets are pre-planned. Such movements should follow a monotonic time-function, and should show a unimodal velocity profile in hand space. We excluded movement trials that presented joint reversals attributed to feedback corrections.
2. All segments were assumed to move simultaneously without staggering between the different joint rotations. By staggering we mean delays at the onset or at the end of the rotation in one joint with respect to the other joints. Underlying this assumption is the idea that different moving segments obey common time constraints.
3. Movements started and ended with zero velocity.

Based on the assumptions above, the main purpose of this work was the comparison between modeled and observed paths for different types of movement.

The Listing's law constraint in extended arm movements

Joint rotations in robotic systems are commonly represented in terms of rotation matrices (Craig 1989). Such a representation has been adopted to describe joint rotations of biological systems in spite of several disadvantages. For example, a matrix representation for rotations involves a high computational cost since it requires the calculation of the three Euler angles. It may also be problematic in some cases since matrices of rotation are non-commutative. Consequently, joint rotations in a reverse order from a final orientation do not bring the joint to the original starting orientation.

On the other hand, in a proper vector representation of rotations non-commutativity is not a concern. Such a representation is suggested for rotations of the eye in the orbit (Tweed and Vilis 1987), and it is deemed relevant for describing internal brain processes such as the representation of the intended direction of the hand movement or the mental rotation of objects (Georgopoulos et al. 1989). A vector representation is compact, computationally more economical and it allows for a suitable formulation of Donders' law under the Listing's law constraint (Haslwanter 1995). Since a representation in terms of rotation vectors seems justified for describing the rotations of the arm segments, we proceed to define rotation vectors of the arm.

Rotation vectors, like rotation matrices, can be used for the description of the orientation of a rigid object (e.g., the limbs) with respect to a given reference configuration. Mathematically a rotation vector is defined as (Hepp 1990; Haslwanter 1995):

$$\vec{r}(\theta, \vec{n}) = \vec{n} \cdot \tan \frac{\theta}{2}, \quad |\vec{n}| = 1, \quad (1)$$

where \vec{n} is a unit vector in the direction of the rotation axis, and θ is the rotation angle around this axis measured with respect to a given reference configuration. It is important to note that the components of the rotation vector depend on the chosen reference position.

The rotation vector of two successive rotations, \vec{r}_1 and \vec{r}_2 , is given by (Hepp 1990):

$$\vec{r}_2 \circ \vec{r}_1 = \frac{\vec{r}_1 + \vec{r}_2 + \vec{r}_2 \times \vec{r}_1}{1 - \vec{r}_1 \cdot \vec{r}_2}. \quad (2)$$

We first focus on extended arm movements with three degrees of freedom at the shoulder joint, which can be defined by the elevation, azimuth and torsion angles, or alternatively by a single rotation vector. In this regard, Listing's law may simplify computations and may allow for a solution to the inverse kinematic problem. In a redundant system such as the human arm, the joint constraint given by Listing's law reduces the number of joint degrees of freedom from three to two since the torsion angle can be obtained from the specific elevation and azimuth angles.

Listing's law defines a constraint in the rotation vector space describing specific arm postures. It states that the rotation vectors with respect to an arbitrary reference position lie within a plane. This strategy implies that the axis of rotation of the upper arm segment is expected to remain fixed in space during the movement (a single-axis rotation, Hepp 1990). As a consequence of a single-axis rotation, the upper arm segment in our model is assumed to rotate in a way that confines the rotation vectors to follow a straight line within Listing's plane (see $\vec{r}(\lambda)$ in Fig. 1a). The implementation of such a strategy might be useful primarily "... for systems that wish to optimize the amplitude of the rotations to and from some centrally located primary position, and keep the orientation constant independent of the path taken" (Vilis and Tweed 1991, p 96). Therefore, under the flat Listing's plane and the single-axis rotation constraints applied on the upper arm rotations it is possible to formulate a model that can predict unique shoulder joint angular paths.

Path predictions in fully extended arm movements

Initially, all rotations are measured with respect to the zero configuration of the arm, which is the configuration where all of the joint angles are equal to zero. For our choice of coordinates, the zero configuration corresponds to an arm posture of a subject pointing straight forward with a pronated arm while maintaining the upper limb co-aligned with the x -axis of the fixed laboratory frame.

For movements with a fully extended arm, the posture of the arm is defined by the hand vector \vec{p} , which

connects the center of shoulder joint with the hand location (Fig. 1b).

It is assumed here that a pointing movement from an initial hand location \vec{p}_a (corresponding to an arm configuration described by the rotation vector \vec{r}_a) to a final hand location \vec{p}_b (corresponding to an arm configuration described by the rotation vector \vec{r}_b) is carried out by rotating the extended arm about the shoulder joint such that the rotation vectors follow a straight line from \vec{r}_a to \vec{r}_b within Listing's plane (Fig. 1a). In fact, the resulting hand movements between pointing targets will be curved in the extrinsic 3D space because of such a straight-line constraint on the joint rotation vectors.

The change in orientation of the arm between the initial orientation \vec{r}_a and the final orientation \vec{r}_b can be described by the following set of rotation vectors:

$$\vec{r}(\lambda) = \vec{r}_a + \lambda(\vec{r}_b - \vec{r}_a), \quad (3)$$

where λ is an arbitrary real-valued parameter in the interval $[0, 1]$ that parameterizes the path in rotation vector space, and \vec{r}_a, \vec{r}_b are elements of Listing's plane.

It should be mentioned that rotation vectors could be constrained to a Listing's plane without following single-axis rotations. That is, rotation vectors within the Listing's plane could follow paths other than straight (e.g., curved paths; see Appendix). In such a case, however, the axis of rotation of the arm would no longer be fixed in space.

A Listing's plane constraint is a 2D fit to the cloud of tips of the rotation vectors obtained for a segment during the movements, and it is referred to as the "displacement surface" (Haslwanter 1995). The vector orthogonal to such a displacement plane is called the primary position vector, which defines the orientation of Listing's plane. This becomes our new reference vector, which is determined for each subject in each movement type. The primary position vector is further used for the calculation of the simulated rotations from point to point. Therefore, from now on we can refer to the primary position in the rotation vector space as the "reference position".

According to Hepp (1990), the rotation vectors described by Eq. 1 can also be represented in terms of a single-axis rotation about the axis \vec{n}_{ab} by the amplitude angle θ (as illustrated in Fig. 1b), resulting in a rotation vector of the form:

$$\vec{r}(\theta) = \vec{r}_{ab}(\theta) \circ \vec{r}_a, \quad (4)$$

where $\vec{r}_{ab}(\theta) = \vec{n}_{ab} \cdot \tan(\theta/2)$.

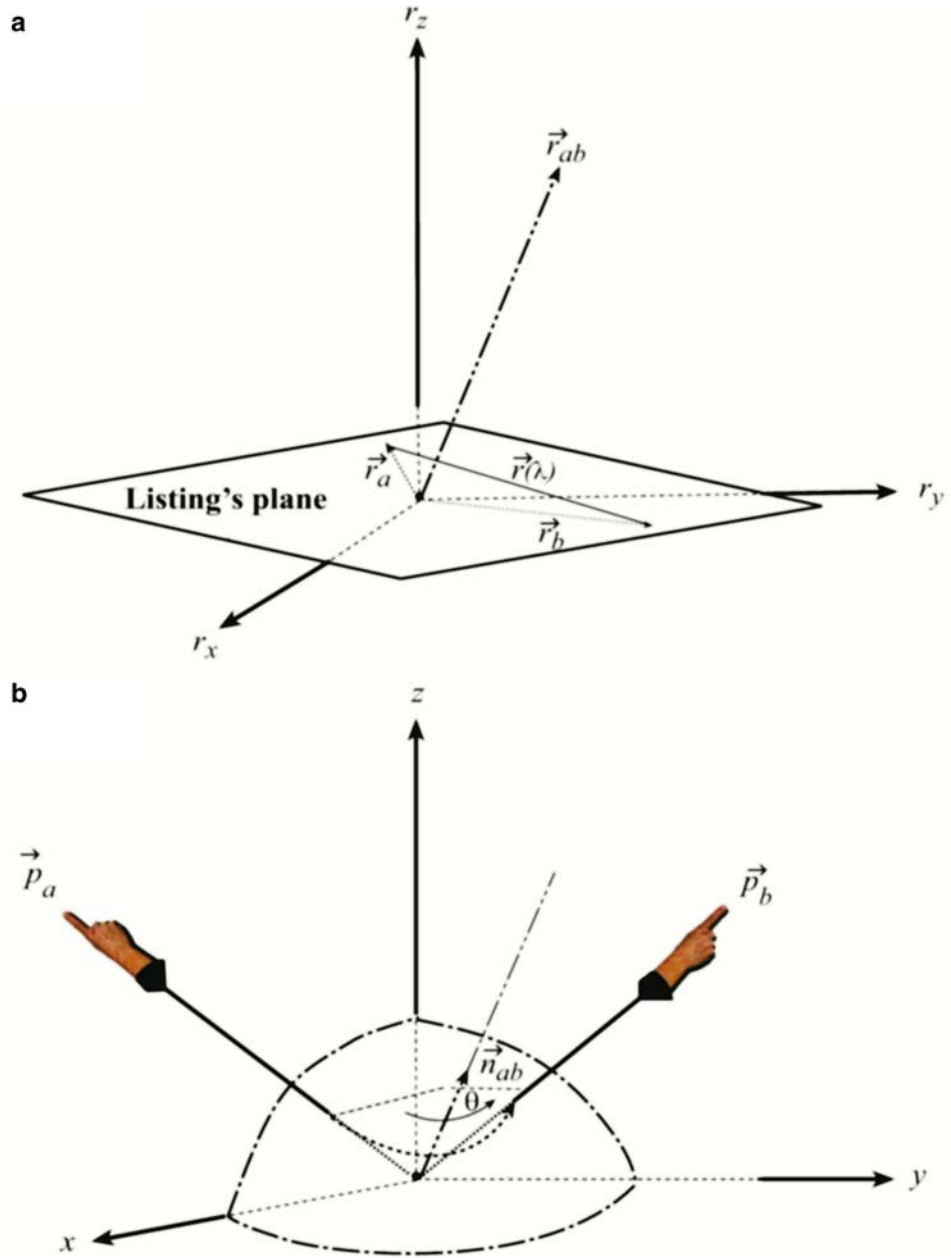
The direction of the fixed axis of rotation is determined by the unit vector:

$$\vec{n}_{ab} = \frac{\vec{r}_{ab}}{|\vec{r}_{ab}|} \quad (5)$$

with the rotation vector

$$\vec{r}_{ab} = \vec{r}_b \circ (-\vec{r}_a) = \frac{\vec{r}_b - \vec{r}_a + \vec{r}_a \times \vec{r}_b}{1 + \vec{r}_a \cdot \vec{r}_b}, \quad (6)$$

Fig. 1 According to Listing's law, three-dimensional joint rotations could be mapped on a flat Listing's plane. In pointing from an initial location \vec{p}_a to another location \vec{p}_b , the rotation vectors of the initial and final arm configurations are defined with respect to a specific reference position called the primary position vector \vec{r}_{pp} which is orthogonal to Listing's plane. **a** Rotation vector space: the straight path $\vec{r}(\lambda)$ in Listing's plane from \vec{r}_a to \vec{r}_b . **b** Hand space: the arm path projected onto a unit sphere, which results from a single-axis rotation around \vec{n}_{ab} by a rotation angle θ from the initial hand location \vec{p}_a to the final hand location \vec{p}_b .



that brings the arm from the initial position \vec{r}_a to the final position \vec{r}_b .

The identity of the rotation vectors given by Eqs. 3 and 4 determines the amplitude angle θ in terms of the path parameter λ . After some algebraic transformations we obtain

$$\theta(\lambda) = 2 \arctan \left(\frac{\lambda(1 + \vec{r}_a \cdot \vec{r}_b) |\vec{r}_{ab}|}{\lambda \vec{r}_a \cdot \vec{r}_b + (1 - \lambda) \vec{r}_a^2 + 1} \right), \quad (7)$$

with the initial and final angles being $\theta(0) = 0$ and $\theta(1) = 2 \arctan(|\vec{r}_{ab}|)$, respectively.

The hand path can be determined from the rotation vector (Eq. 3) according to

$$\vec{p}(\lambda) = \vec{p}_0 + \frac{2}{1 + \vec{r}^2(\lambda)} \{ \vec{r}(\lambda) \times [\vec{p}_0 + (\vec{r}(\lambda) \times \vec{p}_0)] \}, \quad (8)$$

where \vec{p}_0 denotes the hand vector with respect to the reference position.

Path predictions for radial and frontal plane arm movements

Unlike movements that are performed with a fully extended arm, the final hand location in radial and frontal plane movements is determined by rotations about the shoulder and elbow joints. In this case, an arm config-

uration is determined when the rotation vectors of the forearm and upper arm segments are specified. In our simple model, the forearm adds only one degree of freedom about the radio-humeral joint, which describes the flexion–extension movement of the forearm with respect to the upper arm segment.

For radial and frontal movements we assume also that the rotation vector of the upper arm segment follows a straight line within Listing’s plane. Such a rotation vector of the upper arm is given by:

$$\vec{r}_u(\lambda) = \vec{r}_a + \lambda(\vec{r}_b - \vec{r}_a). \quad (9)$$

However, an additional rule has to be applied in order to determine the rotation vector of the forearm. We assume that the flexion–extension rotation β of the elbow joint changes linearly with the amplitude of shoulder rotation θ , leading to the relation

$$\beta(\theta) = \frac{\beta_f - \beta_0}{\theta_f - \theta_0}(\theta - \theta_0) + \beta_0, \quad (10)$$

where θ_0 , θ_f and β_0 , β_f denote the initial and final angles of β and θ , respectively.

An initial support for the linear relation between these two contiguous arm joints (as expressed in [10]) comes from Marotta et al. (2003). These authors have found that the changes in orientation of the upper arm and those of the forearm are linearly related during reaching movements for grasping pre-oriented objects. These changes closely follow Donders’ law. Also, our own findings in 3D pointing movements showed that the rotation angle θ representing the rotation of the upper arm segment about the fixed axis in space and the actual elbow rotation angle β are linearly related during the transport of the hand to the visual targets. Earlier evidence suggesting a linear relationship between the shoulder and the elbow joints was reported by Soechting and Lacquaniti (1981) for actual orientation angles during radial movements toward targets located on a vertical plane and by Hollerbach and Atkeson (1986) during vertical movements carried out within the sagittal plane.

Under the linear assumption, the rotation vector of the forearm with respect to the upper arm segment can be written as:

$$\vec{r}_{fu} = \vec{n} \cdot \tan\left(\frac{\beta(\theta)}{2}\right), \quad (11)$$

where \vec{n} is in the direction of the elbow joint axis in the reference configuration, and β is the flexion angle measured with respect to the extended arm. Note that the flexion angle β can be expressed in terms of the parameter λ by inserting Eq. 7 into Eq. 10.

Finally, the rotation vector of the forearm with respect to the reference position can be expressed as:

$$\vec{r}_f = \vec{r}_u \circ \vec{r}_{fu}. \quad (12)$$

The elbow and the hand paths are determined by the rotation vectors of the forearm and upper arm segments. The elbow path is given by:

$$\vec{p}_e(\lambda) = \vec{p}_{e,0} + \frac{2}{1 + \vec{r}_u^2(\lambda)} \{ \vec{r}_u(\lambda) \times [\vec{p}_{e,0} + (\vec{r}_u(\lambda) \times \vec{p}_{e,0})] \}, \quad (13)$$

and the hand path is given by:

$$\vec{p}_h(\lambda) = \vec{p}_e(\lambda) + \vec{d}_0 + \frac{2}{1 + \vec{r}_f^2(\lambda)} \{ \vec{r}_f(\lambda) \times [\vec{d}_0 + (\vec{r}_f(\lambda) \times \vec{d}_0)] \}, \quad (14)$$

with $\vec{d}_0 = \vec{p}_{h,0} - \vec{p}_{e,0}$, where $\vec{p}_{e,0}$ and $\vec{p}_{h,0}$ are the elbow and the hand locations in the reference position.

It should be noted that relations (13) and (14) reduce to the expression in Eq. 8 for $\beta = 0$, when the arm is fully extended.

The above modeling process is summarized schematically in Fig. 2.

Finally, the model based on Listing’s law presented here makes no predictions concerning the evolution of the movement over time. Such a model is limited to describing the geometrical characteristics of the paths. The temporal aspects of the movement could easily be included in our framework by modeling the temporal development of the rotation angle θ around the fixed axis of rotation.

Materials and methods

Subjects and apparatus

Four right-handed male individuals (age range 18–32 years old) completed a series of natural reaching and pointing movements of different types. The data were collected via an Optotrak motion capturing system (Northern Digital, Inc., Waterloo, ON, Canada) at a sampling rate of 100 Hz. Joint rotation vectors and end-point trajectories were off-line calculated using a series of custom-made subroutines written in Matlab code (MathWorks, Natick, MA, USA). Detailed descriptions of our subjects and the apparatus are provided in the accompanying manuscript.

Experimental procedures and design

The experiment consisted of a series of hand movements toward 3D virtual targets presented sequentially at different locations within the 1 m × 1 m × 0.8 m workspace. All four participants completed the set of trials. Modeled end-point kinematic data were compared with the empirical data obtained in the following experimental conditions:

1. Extended arm pointing: movements that started from 24 different locations and were performed toward one final target position (one set). A set of movements was repeated five times for each of nine possible final target positions (24 movements × 9 sets × 5 times = 1,080 trials per subject).

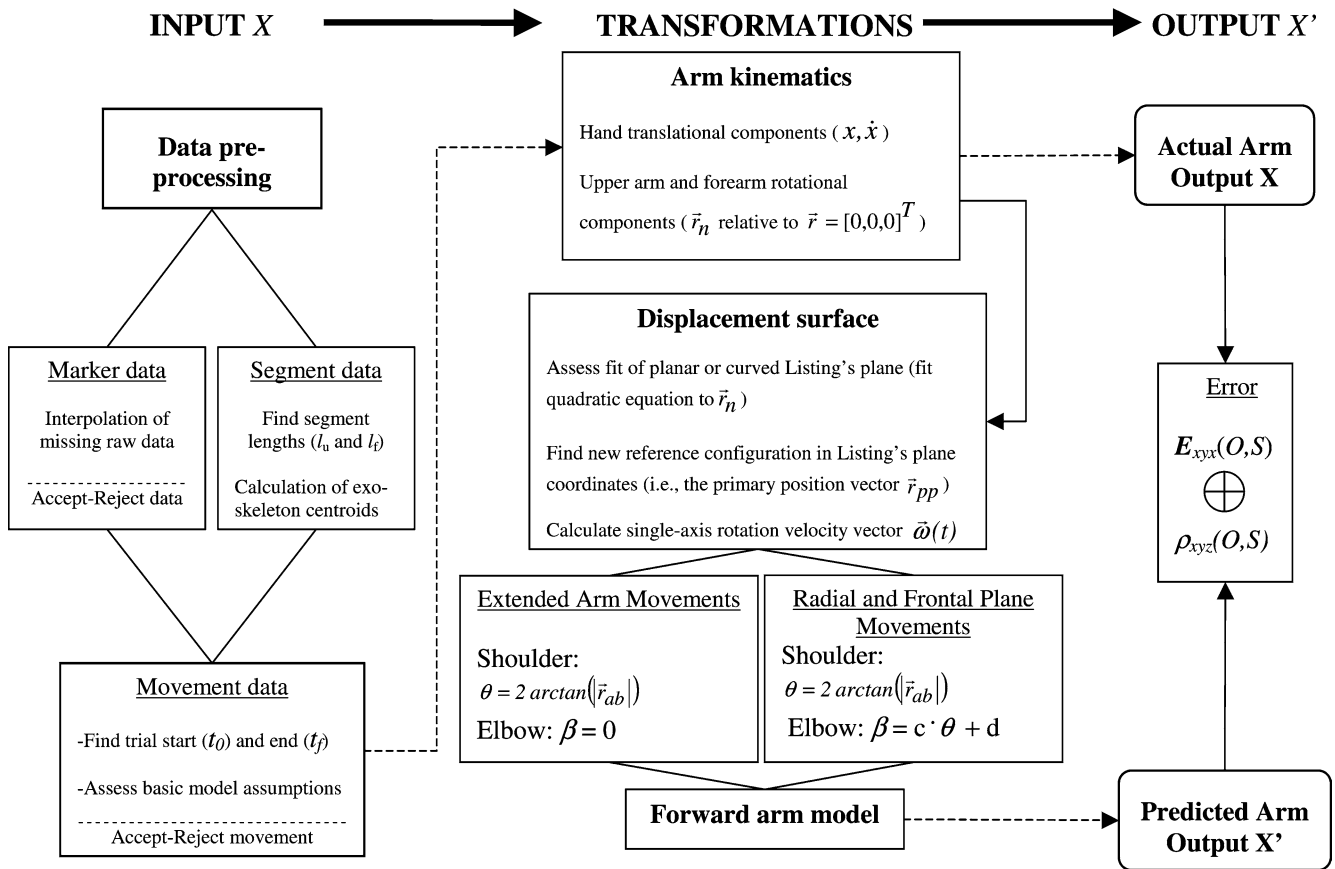


Fig. 2 Schematic diagram showing the processes involved in the data analysis and modeling approach under the constraint of Listing's law. *Arrows* indicate the flow of the process. *Black lines* refer to internal subprocesses within a stage while *dashed lines* are used to represent data transfer from one stage to another (Input X , Transformations, Output X') once the computations in the previous stage are completed. After the marker data were pre-processed, segmental data were calculated (the centroids for the wrist, elbow, and shoulder exo-skeletal frames, upper arm length l_u and forearm length l_f). A preliminary movement analysis followed. Arm kinematics were then calculated (translational: displacement x and velocity \dot{x} ; rotational: rotation vectors \vec{r}_n and single-axis rotation vectors \vec{r}_{ab}). The single-axis angular velocity vectors $\vec{\omega}(t)$

were calculated using the \vec{r}_n vectors. Best fitting surfaces (i.e., Listing's planes) were found for the distributions of the tips of the rotation vectors \vec{r}_n . The vector \vec{r}_{pp} (orthogonal to the best fitting plane) was defined as the new reference configuration in Listing's coordinates. The angle θ parameterized the rotations of the shoulder relative to \vec{r}_{pp} , while the angle β defined the rotation angle of the elbow joint relative to the upper arm. Finally, data were compared in terms of the differences between the observed (O) and the simulated (S) paths. Absolute differences between the observed and the simulated paths were assessed by calculating mean squared errors $E_{xyz}(O,S)$ while differences in shape between the paths were examined using correlation coefficients $\rho_{xyz}(O,S)$

2. Radial reaching: movements that started from a fixed region (0.4 m from the shoulder) toward 39 different final target positions at a distance of 0.6 m from the shoulder for short movements or at a distance of 0.8 m for long movements. This was also repeated five times (2 frontal depths \times 39 movements \times 5 times = 390 trials per subject).
3. Frontal plane reaching: movements performed in one of two fixed fronto-parallel planes at distances of either 0.30 or 0.60 m relative to the trunk. For the present analyses, the movements taken into consideration started from six different locations and ended at one of six final target locations, all confined to the same plane. This was repeated five times until completing the sets (2 fronto-parallel planes \times 6 final target locations \times 6 movements \times 5 times = 360 movement trials per subject).

Kinematic data were calculated from at least three infrared emitting diodes (IREDS) of the four IREDS markers attached to each segment. A computer algorithm was used to detect trials that markedly violated the assumptions made about the arm kinematics. Such trials included, for example, movements in which the elbow and shoulder rotations did not start and end together (i.e., within a time window of 20 ms), or when the joint angular velocity was $> 10\%$ of the peak speed at the start or at the end of the movement for a period of $> 10\%$ of the movement time. Movement trials that showed major shoulder reversals were not taken into consideration either.

A linear relationship between the single-axis rotation of the shoulder and the elbow flexion-extension was assumed. This joint relationship was assessed for radial movements and frontal plane movements. A

trial was eliminated only when the linear assumption was grossly violated at the end or at the start of the movement. The experimenter occasionally re-evaluated some of those trials in an attempt to recover them (e.g., when a minor end-point reversal was observed or when the velocity profile showed multiple minor peaks at the start or at the end, as shown in Fig. 3a, b). If there were missing data points at movement onset or at the end of the movement, the data were extrapolated to the zero velocity level based on a superposition of a minimum-jerk speed profile fitted to the tangential end-point velocity. The best fit was computed by minimizing the squared error between the observed velocity data and the superimposed minimum-jerk speed profile (Lee et al. 1997). Figure 3 illustrates such a process for two different movement examples.

The percentage of trials that were automatically detected as “correct”, “staggered”, and “reversal” is shown in Fig. 4. Approximately 35% of the total number of movements was rejected. A large portion of these rejected trials resulted from erroneous performances and not from violations of the basic assumptions. For example, subjects were sometimes unable to move between targets within the specified inter-trial intervals (1.5 s). A delay in the initiation of one movement could affect the following one in the sequence. Additional errors could occur when the subjects were uncertain about the depth of the perceived virtual object or when they failed to pay attention to the task.

It is worth to note that objective criteria and quality restrictions were equally applied to all trials and movement types, in a random and blind manner. Therefore, the percentage of rejected trials was quite homogeneous among all three types of movements (Fig. 4), and the normal distribution was not violated. Even though the percentage of rejection was quite significant, the number of movement trials still left for the analyses was large because of the large amount of data initially collected.

Analysis

The main analysis consisted of a comparison between the predicted paths and the experimental end-point paths. Raw marker data were off-line processed to obtain 3D Cartesian coordinates of the forearm and upper arm segments. Listing’s planes were calculated for each participant in all repeated sets of pointing movements of three types. These reference planes served to define primary position vectors \vec{r}_{pp} . For each subject, we obtained mean \vec{r}_{pp} vectors (i.e., the mean of five repetitions of the same sets of movements) for nine extended arm movement levels corresponding to the nine final target positions, for the long- and short amplitude radial movements, and for 12 levels in frontal plane movement-type that corresponded to

reaching movements toward six final target positions in two different fronto-parallel planes. For the simulation of rotations from point to point, a grand mean \vec{r}_{pp} was used as the reference position derived from a look-up table of local primary position coordinates. This defined one flat Listing’s plane per subject for each movement type.

The start and final end-point coordinates of the hand in space (\vec{p}_a and \vec{p}_b) were relative to a coordinate system whose origin was located at the shoulder. The upper arm (l_u) and the forearm (l_f) lengths were determined using the IRED marker data. The length l_u was defined as the distance from the center of the shoulder markers to the center of the elbow markers. The length l_f was defined as the distance from the center of the elbow markers to the center of the markers attached the dorsal side of the hand-wrist system. Shoulder and elbow rotations were then calculated from the marker data, and further converted to rotation matrices, rotation vectors, and angular velocity vectors. The best fitting planes were calculated based on the rotation vectors.

The differences between the simulated and the real movements were statistically analyzed by using within-subject analyses of variance (RM-ANOVA). A JMP-2 package (SAS Institute Inc., Cary, NC, USA) was used for the ANOVAs. Cross-correlation coefficients and absolute error estimates were used to quantify the discrepancies between the simulation results and the experimental observations. These variables were computed as follows:

1. The numerical estimate of the fit for an observed curve O and its corresponding simulated curve S was calculated using the correlation coefficient ($\rho(O,S)$) given by:

$$\rho(O,S) = \frac{1/n \cdot \sum_{i=1}^n (O_i - \bar{O}) \cdot (S_i - \bar{S})}{\sqrt{1/n \cdot \sum_{i=1}^n (O_i - \bar{O})^2} \cdot \sqrt{1/n \cdot \sum_{i=1}^n (S_i - \bar{S})^2}},$$

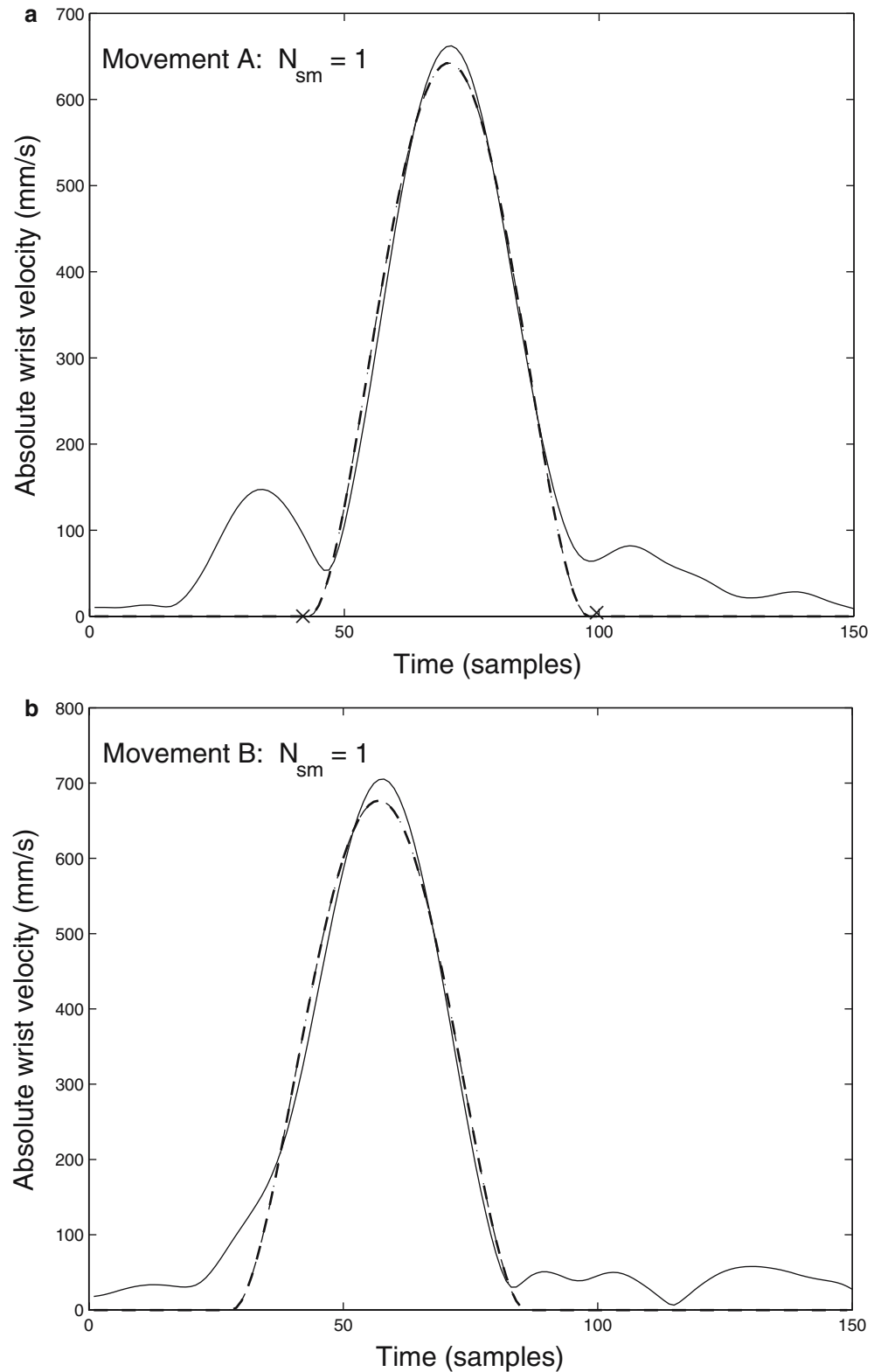
where n is the number of samples of O and S . For an optimal fit between the observed and modeled sequences, $\rho(O,S) = 1$. The correlation is calculated for the paths projected on the three planes. The coefficients obtained are then averaged and used as an estimate of the 3D fit between the observed and simulated end-point paths.

2. The error term is calculated using the root mean square differences between simulated and discrete observed paths according to the following formula:

$$E(O,S) = \sqrt{1/n \cdot \sum_{i=1}^n (O_i - S_i)^2},$$

where n is the number of samples, S the simulated model data and O the observed data.

Fig. 3 Estimation of the onset and end of a movement at zero velocity levels using an extrapolation method that is based on the minimum-jerk polynomial. The experimenter visually defined the limits of the major unimodal symmetric velocity profile, as indicated by marker 'x' on the time-axis. The number of minimum-jerk submovements (N_{sm}) assumed within a movement trial was $N_{sm} = 1$. The example at the *top* shows an acceptable estimate of the time of onset at zero end-point tangential velocity. However, the estimate achieved by the algorithm was not quite right for the end of the movement. The example at the *bottom* shows a successful estimate for the end of the movement, but not as good an estimate for the time of onset. The experimenter visually redefined the end of the movement (or its onset) in cases such as the bottom example. The trial was rejected when an educated guess did not lead to a satisfactory extrapolation to the assumed zero velocity level

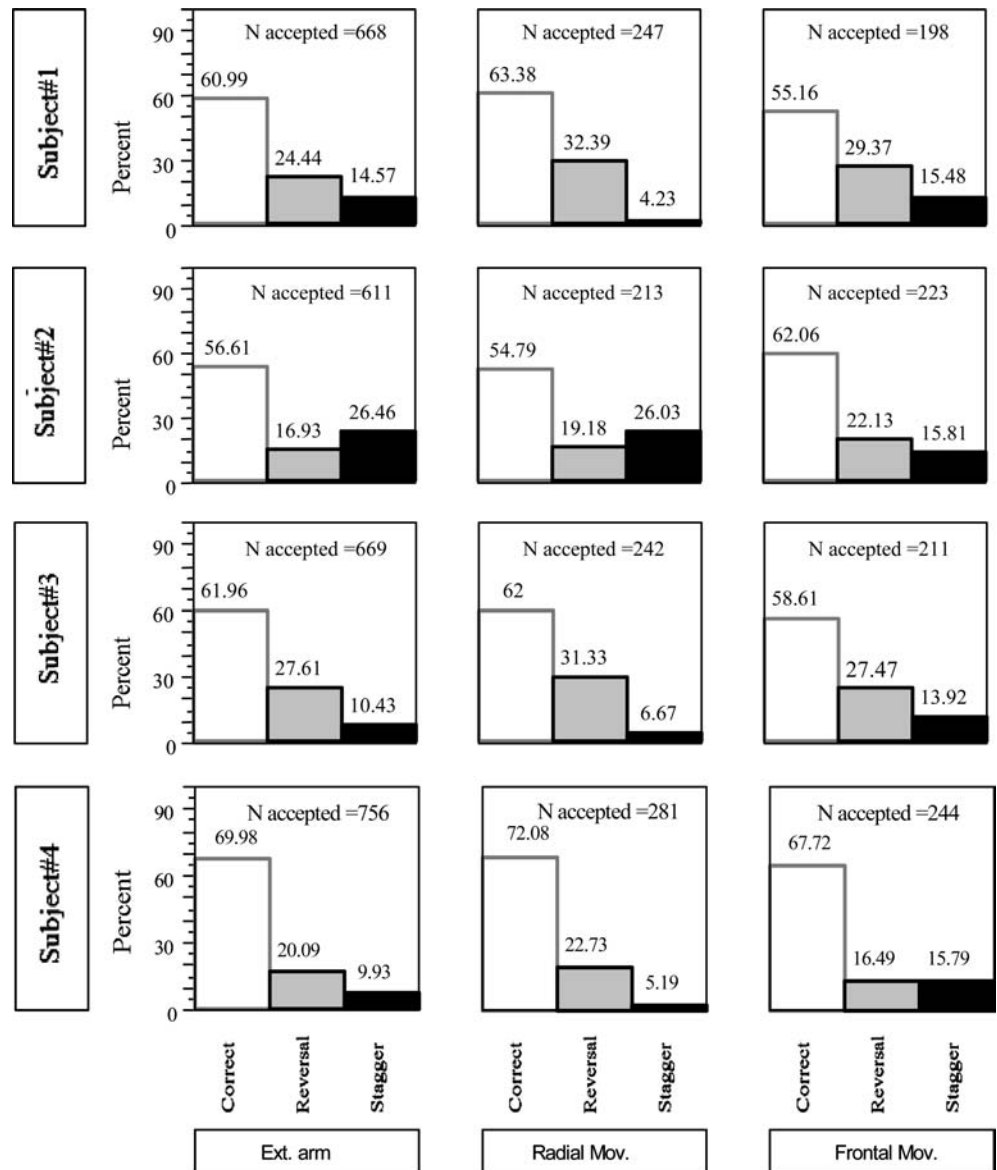


This error analysis is independently applied to the projections of the hand path into the x - y , x - z , and z - y planes. A total error estimate is obtained by taking the mean of these values,

$$E_{xyx}(O, S) = 1/3 * [E(O_{xy}, S_{xy}) + E(O_{xz}, S_{xz}) + E(O_{zy}, S_{zy})].$$

For all statistical analyses, the confidence level was set at $P \leq 0.05$.

Fig. 4 Proportion of trials (in percentages) coded by the computer algorithm as “correct” (white columns), “reversal” (gray columns), and “staggered” (black columns) in the three different movement types and for our four subjects. Reversal trials were characterized by sudden shoulder or elbow flexion–extension movements during the hand transport to the pointing target. Staggered trials were those for which the elbow or shoulder joint started rotating out of phase relative to each other. Correct trials were those that followed the basic model assumptions. Note that the number of accepted trials (N) does not include movements that were re-assessed and which were eventually included in the analyses



Results

Linear relationship between the θ angle around the single-axis for the rotations of the upper arm and the β angle for the flexion–extension of the elbow

A regression line was fitted to the angle–angle plots of the θ angle of the shoulder joint rotation vs the β angle of the elbow joint rotation, in the radial and frontal plane movements. This was carried out to assess the linear relationship between these two particular joint rotations. The results suggested that the linear assumption was valid for the portion of the path that corresponded to the transport phase of the hand to the target. High correlation coefficients were obtained for the linear fit in approximately 62% of the trials. For radial movements the mean correlation coefficient (ρ) and the SD around the mean correlation were $\rho = 0.95 (\pm 0.066)$

for subject #1, $\rho = 0.94 (\pm 0.076)$ for subject #2, $\rho = 0.95 (\pm 0.071)$ for subject #3 and $\rho = 0.95 (\pm 0.066)$ for subject #4, all significant at $P < 0.001$. Deviations from the linear fit were occasionally observed at the end of the movement, presumably because the last portion of the path was dependent on visual feedback. Close to the virtual target, one of the joints stopped moving while the other still rotated in order to increase pointing accuracy.

Posture of the arm during point-to-point movements

Our model was designed to predict the 3D end-point paths that result from constraining the upper arm segment to postures that obey Listing’s law. Generic arm postures generated by our model are presented in Fig. 5a–c.

It should be noted that, as a by-product of the single-axis shoulder rotations, the resulting 3D paths of the elbow are likely to be curved.

End-point paths after constraining arm joints to follow Listing's law

The following plots show examples of simulated vs observed paths in the three movement types studied here (Fig. 6a–c).

Figure 6a shows a series of pointing movements toward different locations in space with an extended arm. Note that when the arm is fully extended, there is a close match between the simulated paths and observed end-point paths. With a few exceptions, this pattern was common for all subjects in all sets of extended arm movements.

Examples shown in Fig. 6b are representative of large-amplitude radial movements. In this movement type, deviations from the model predictions were more frequent regardless of the direction of the movement. A possible explanation for such deviations could be found in the violations of the flat Listing's plane assumption. The upper arm rotation vectors in this movement type tended to fit curved surfaces, depending on the amplitude of the rotation. In contrast to the previous movement types, the discrepancies between the observed and predicted movements during frontal plane movements appeared to be larger and more frequent (Fig. 6c).

Quantification of the above observations is presented in the following paragraphs in terms of the differences in the shape and the mean squared differences between the simulated and experimental paths.

Differences between modeled and observed paths

Similarities and differences between the predicted and experimental data can further clarify whether or not our model predicted the actual paths. Modeled vs observed end-point paths for each trial were compared by calculating the error E_{xyz} , independently for the three planes of projection of the 3D movements. These values were averaged to obtain an estimate of the differences between the simulated and recorded paths. E_{xyz} values were used as the dependent variable in an analysis of variance that showed that subjects differed from each other ($F_{(3,50)} = 3.49$; $P = 0.015$). The "Movement type" factor showed a significant effect ($F_{(2,50)} = 17.42$; $P < 0.001$) in that extended arm movements resulted in smaller modeled–observed path differences than radial movements. Radial movements, in turn, resulted in smaller modeled–observed differences than frontal plane movements.

It should be kept in mind that frontal plane movements had larger d , e , and f coefficients than other types of movement (rotation surfaces were

twisted), but the SD values around the fitted surfaces were not significantly larger compared to those found for other movement types (see Liebermann et al. 2005, manuscript I). Thus, for frontal plane movements the deviations of the observed paths from the modeled paths are likely to be explained by the discrepancy between the assumed flat Listing's plane and the actual twisted surfaces that best fitted these data. Further interpretation of the amount of success or failure of the model in predicting realistic movements will be dealt with in the section Discussion for this and the other movement types.

Effects of movement direction on modeled–observed E_{xyz}

Extended arm movements were carried out from 24 different starting locations toward one single final target in each set. This was repeated for nine different final target locations. Listing's planes were determined for movements directed toward each of the nine final targets independently, but a mean primary position derived from these Listing's planes was used to calculate movement paths. The analysis on the differences between end-point paths using the root mean square difference (E_{xyz}) as the dependent variable showed a major effect of the final "Target location" ($F_{(8,169)} = 6.05$; $P < 0.001$). Post hoc pairwise comparisons showed that movements toward position #1 (upper left corner), position #5 (the center of the workspace) and position #9 (lower right corner) resulted in non-significant differences between the predicted and measured paths compared to the other final locations.

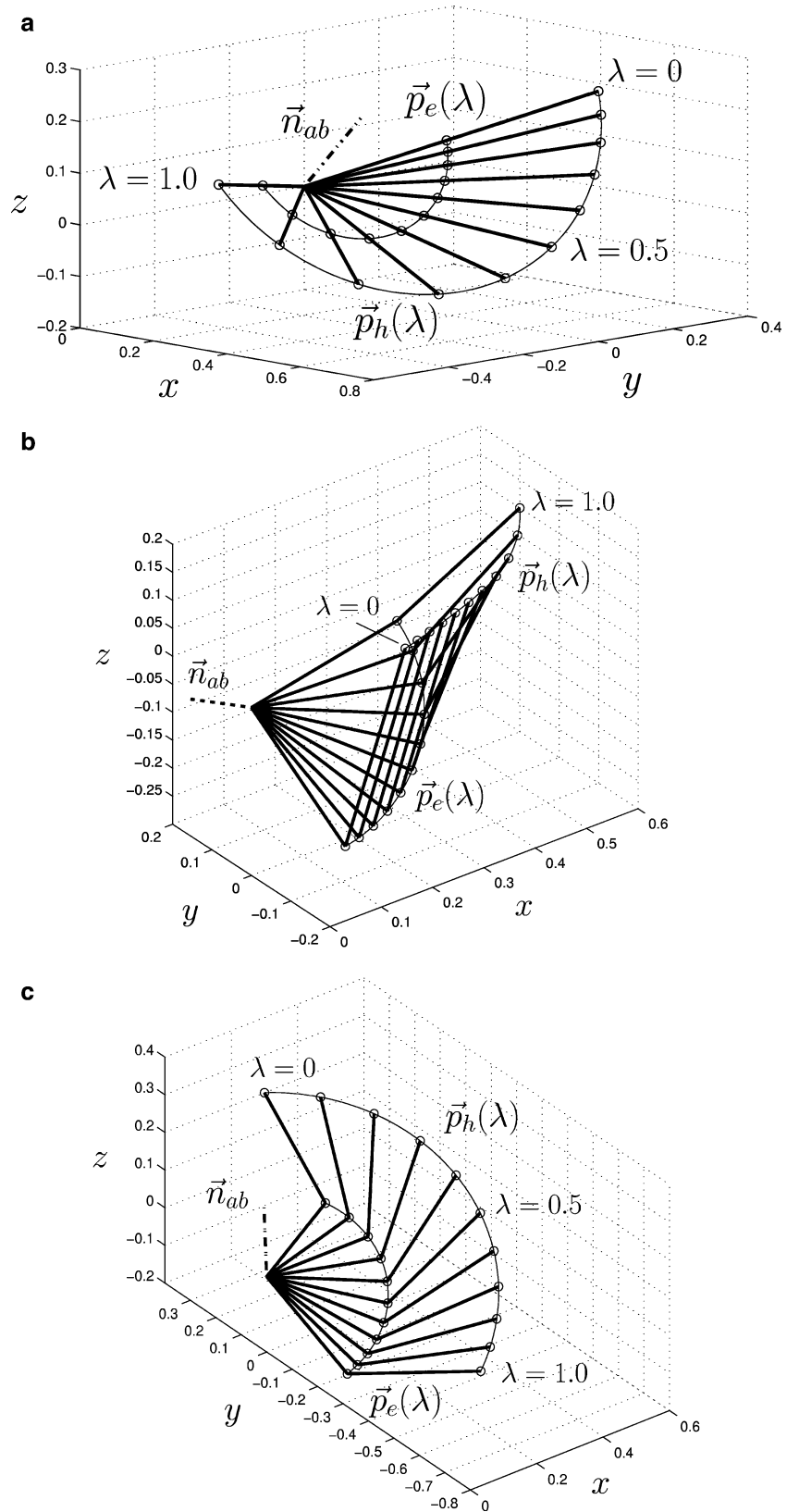
Effects of movement size on the modeled–observed E_{xyz}

In this case, long- and short-radial reaching movements were analyzed separately and two Listing's planes were calculated for each subject from the repeated sets of trials in long and short amplitude reaching. The results showed that the observed–modeled differences increased for large movements as compared to small amplitude movements (mean E_{xyz} for large = 14.01; mean E_{xyz} for short = 11.29). Such differences achieved statistical significance ($F_{(1,38)} = 6.07$; $P = 0.014$).

Evaluation of modeled–observed path differences by correlation analyses

The data were also assessed in terms of the correlation between the modeled and the observed trajectories. Mean cross-correlation coefficients $\rho(O,S)$ were used as the dependent variable in an ANOVA. The ANOVA showed a major effect for the "Subjects" factor ($F_{(3,50)} = 19.65$; $P < 0.001$). The coefficients for extended arm, radial and frontal plane movements slightly

Fig. 5 The illustrations show simulated arm postures (for the forearm–upper arm link) for different values of the path parameter $\lambda = 0.0, 0.1, \dots, 1.0$, in three movement type categories. *Thin lines* describe the end-point paths of the hand $\vec{p}_h(\lambda)$ and the elbow $\vec{p}_e(\lambda)$ at ten step-values of λ (empty dots). The paths result from constraining the shoulder to rotate about a constant axis given by \vec{n}_{ab} (dashed line) and from imposing a linear constraint on the rotations of the elbow and shoulder joints. The initial and final target locations were given by $\vec{x}_0 = l_u(\cos(30^\circ) \sin(70^\circ), \sin(30^\circ) \sin(70^\circ), \cos(70^\circ))$ and $\vec{x}_f = (l_u + l_f)(\cos(-60^\circ) \sin(80^\circ), \sin(-60^\circ) \sin(80^\circ), \cos(80^\circ))$, respectively. The assumed upper arm length $l_u = 0.30$ m and the forearm length $l_f = 0.32$ m. **a** The top figure shows the simulated path of an extended arm movement using the following parameters: initial target location $\vec{x}_0 = (0.505, -0.291, 0.212)$; final target location $\vec{x}_f = (0.305, -0.529, 0.108)$; initial rotation vector $\vec{r}_a = (1.7892, 0.2749, 0.5964)^T$; final rotation vector $\vec{r}_b = (0.0001, -0.1162, -0.5727)^T$; initial flexion angle $\beta_0 = 0^\circ$; final flexion angle $\beta_f = 0^\circ$. **b** The middle figure shows the simulated path of a radial arm movement. The parameters used were $\vec{x}_0 = (0.3, 0, 0)$; $\vec{x}_f = (0.6, 0.1, 0.1)$; $\vec{r}_a = (0.7668, 0.4837, -0.6299)^T$; $\vec{r}_b = (0.0891, -0.0701, 0.0336)^T$; $\beta_0 = 122.2^\circ$ and elbow $\beta_f = 12.3^\circ$. **c** The bottom figure presents the simulation result of a frontal plane movement. In this case, the parameters were $\vec{x}_0 = (0.3, 0.4, 0.2)$; $\vec{x}_f = (0.3, -0.45, -0.15)$; $\vec{r}_a = (0.2737, -0.0198, -0.2349)^T$; $\vec{r}_b = (0.6539, 0.0210, -0.9877)^T$; $\beta_0 = 59.4^\circ$ and elbow $\beta_f = 50.3^\circ$. Note that in frontal movements the targets at the start and the end lie in the same plane



differed from each other ($\rho(O,S) = 0.929, 0.925, \text{ and } 0.918$, respectively), but these differences did not achieve a statistical significance ($F_{(2,50)} = 2.98$; $P = 0.051$). The

“Subjects” and “Movement type” factors interacted ($F_{(11,50)} = 3.339$; $P = 0.003$), most likely because subjects significantly differed from each other.

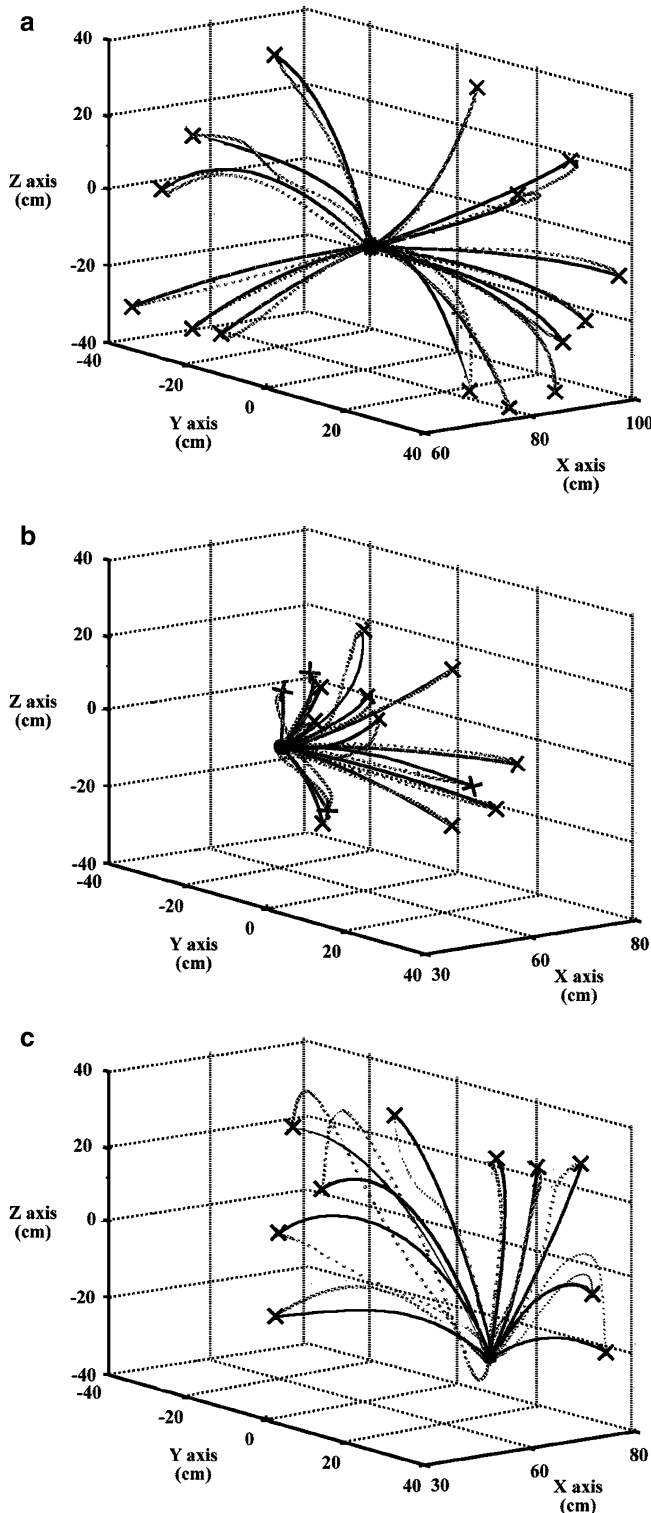


Fig. 6 Randomly chosen examples of three-dimensional simulated paths (line), as predicted by the model vs the observed end-point paths (dots) during: **a** fully extended arm movements, **b** radial arm movements, and **c** frontal plane arm movements performed to one final target (x , y , and z coordinates in meters) from different starting locations

Results on the directional constancy of the single-axis angular velocity vector

As suggested in the Theoretical Model section, rotations were assumed to be about a single axis and therefore the angular velocity vector $\vec{\omega}(t)$ was assumed to maintain a constant direction under the constraint of Listing's law (Hepp 1990). This implies that the transition from \vec{r}_a to \vec{r}_b should follow a straight-line path within Listing's plane. However, the suitability of the flat Listing's plane constraint in some movement types does not preclude the possibility that differences between the modeled and the observed paths could be caused by a change in the direction of the axis of rotation of the upper arm during a movement, or likewise by changes in direction of the single-axis angular velocity vector $\vec{\omega}(t)$.

We calculated $\vec{\omega}(t)$ vectors using Eq. 15 in the Appendix. The directional constancy of $\vec{\omega}(t)$ is quantified, but since $\vec{\omega}(t) = (\omega_x(t), \omega_y(t), \omega_z(t))$, the mean and SD values were calculated for each component. The $\vec{\omega}(t)$ data (in rad/s) of each movement trial were smoothed using a median running time-window of three samples. For comparison purposes, they were normalized to maximum. A coefficient of variation (CV) was obtained from the ratio $CV(\omega_i) = |SD(\omega_i)/Mean(\omega_i)|$, $i = x, y, z$, independently for $\omega_x(t)$, $\omega_y(t)$, and $\omega_z(t)$. A mean homogeneity factor $\bar{H}(\vec{\omega}) = 1/3 * [CV(\omega_x) + CV(\omega_y) + CV(\omega_z)]$ was then computed and used as an estimate of the directional constancy of $\vec{\omega}(t)$. $\bar{H}(\vec{\omega})$ values near zero would indicate relative directional constancy of the axis of the angular velocity vector.

Figure 7 shows typical examples of the results obtained for the $\vec{\omega}(t)$ vectors.

A plain visual inspection of any set of trials led to the conclusion that $\vec{\omega}(t)$ does not keep a constant direction. This was confirmed by the $\bar{H}(\vec{\omega})$ results, which showed values significantly different from zero. Only a few movements showed low $\bar{H}(\vec{\omega})$. The mean homogeneity factor $\bar{H}(\vec{\omega})$ for the different types of movement was 0.996 (SD ± 0.448 , median 0.924) for extended arm movements, 0.966 (SD ± 0.453 , median 0.88) for radial movements and 1.034 (SD ± 0.450 , median 0.989) for the frontal plane movements. Although, $\vec{\omega}(t)$ vectors in frontal plane movements were the least constant, analyses showed that differences in $\bar{H}(\vec{\omega})$ among movement types were not significant ($P = 0.137$). Distribution plots of $\bar{H}(\vec{\omega})$ vectors in each movement type are presented in Fig. 8.

Discussion

Different neural substrates are responsible for specifying the posture of the arm during the transport phase and for grasping an object (Humphrey 1979). This is also

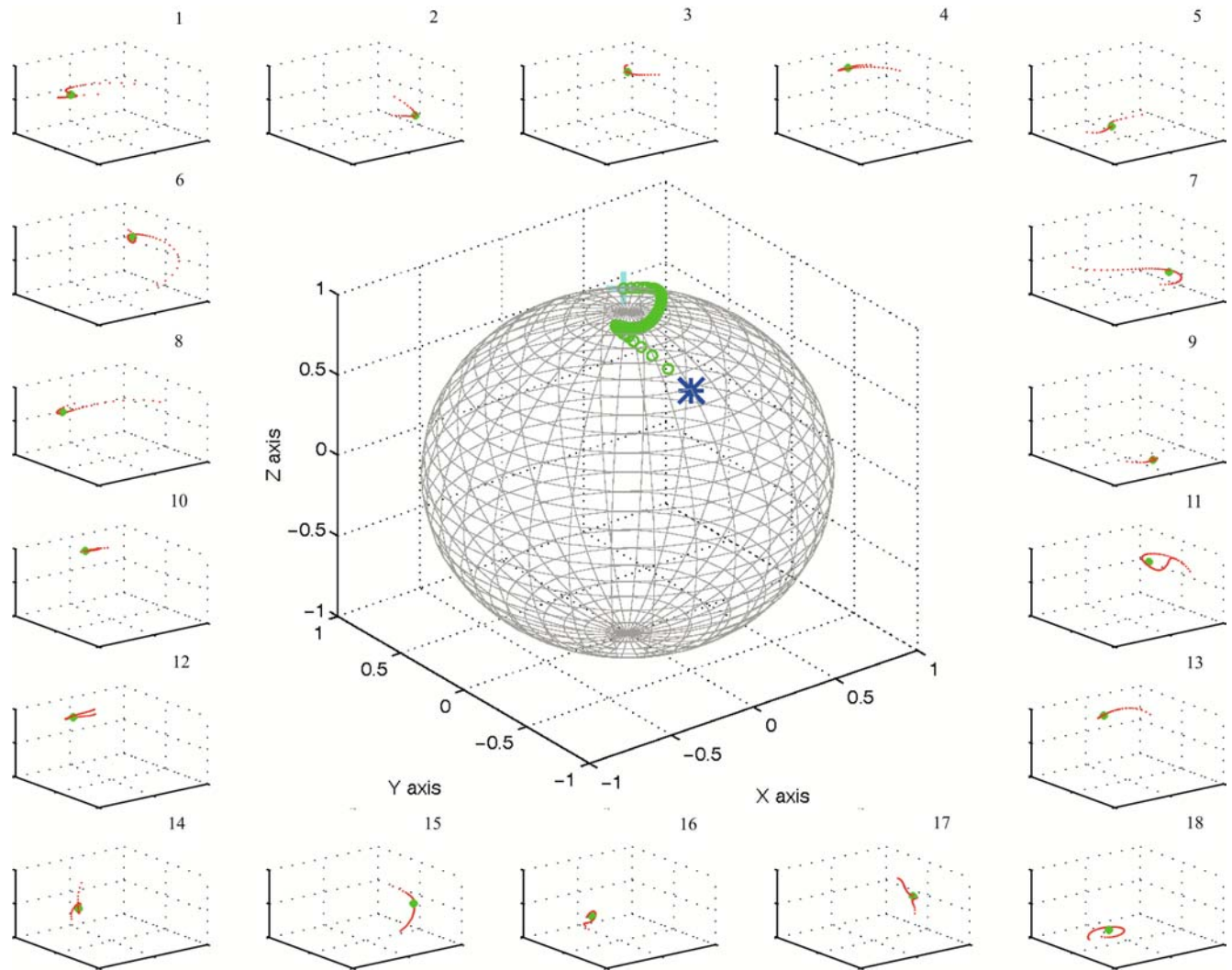


Fig. 7 Examples of three-dimensional angular velocity vectors $\vec{\omega}(t)$ for the shoulder joint during extended arm movements (*dotted line*) expressed in normalized units (NU) for comparison purposes only. The *dot-start* in the zoomed illustration in the center represents the end of the movement; the *dot* in each small plot

represents the median value of $\vec{\omega}(t)$. The examples show that $\vec{\omega}(t)$ vectors do not maintain constant axes. A similar observation was made regardless of the performer, amplitude, direction, or type of movement

evident at the arm kinematic level (Jeannerod 1988, 1990). In the present investigation, we have focused on the transport of the hand towards a target. Some authors have argued that transporting the hand in a point-to-point movement is planned in extrinsic coordinates (Flash and Hogan 1985; Wolpert et al. 1995). Others have suggested that intrinsic joint coordinates could be used (Flanagan and Ostry 1989).

In line with the latter view, we have introduced Listing's law as a relevant constraint for the rotations of the upper arm segment about the shoulder. We assumed that a flat Listing's plane dictates the arm orientation under the constraint of a constant axis of rotation (i.e., rotations of minimal amplitude), and consequently, this was expected to dictate also the extrinsic hand paths.

We compared simulation results with experimental results. These results were expected to bring about some insights into meaningful intrinsic kinematic

planning strategies used by the brain. However, this could only be realized under the assumption that the motor plans for achieving the desired motor execution schemes are not too strongly affected by the movement dynamics, or by assuming that the motor system has an accurate internal representation of arm dynamics in order to compensate for possible distortions. In our kinematic modeling approach, such dynamic effects were not considered.

Previous studies investigated the relevance of Listing's law for the arm (Straumann et al. 1991; Hore et al. 1992; Miller et al. 1992; Crawford and Vilis 1995). In general, Listing's law appears to be obeyed, although it has been pointed out that its implementation may depend on several factors that determine the degree of curvature or twist of the Listing's rotation surface. For example, the type of motor task that is being performed and its goal (Hore et al. 1994; Ceylan et al. 2000), the

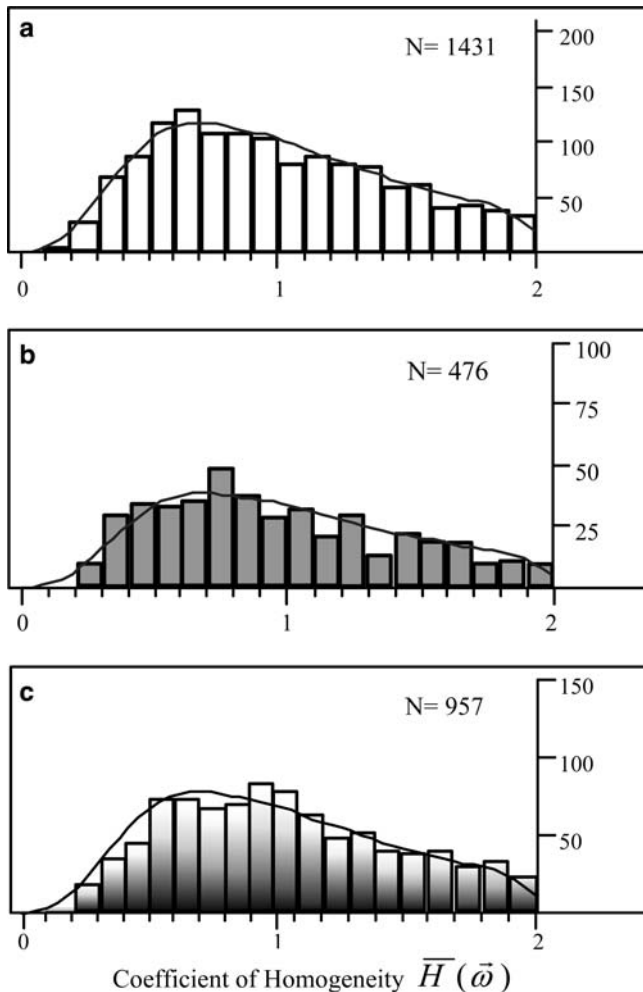


Fig. 8 The plots for **a** extended arm, **b** short amplitude radial, and **c** frontal plane movements show the frequency distributions of the $\bar{H}(\bar{\omega})$ for N number of trials. Clearly, only a few of the movements collected showed values close to zero

specific kinematic requirements of the task (Admiraal et al. 2001), and the context in which the movement is carried out (Medendorp et al. 2000).

The findings reported in the accompanying manuscript (Liebermann et al. 2005) suggested that the type of movement carried out affected the suitability of a Listing's plane constraint. This might have a partial influence on the results in this second part of our study. Frontal plane movements, for example, showed large discrepancies between experimental and modeled paths perhaps because the flat Listing's plane assumption was the least suitable for such a type of movement. This was not the case for radial movements because the results showed a reasonable degree of correspondence between simulated and experimental paths. Yet, the shoulder rotations in radial movements somewhat deviated from the flat Listing's law constraint and fitted curved planes but curvature for these planes was inconsistent and chan-

ged as a function of the amplitude of the rotation. As a consequence, short radial movements presented a reasonably good degree of correspondence between simulated and experimental paths. For extended arm movements, the upper arm rotation vectors fitted two-dimensional surfaces which were very close to a flat Listing's plane ($< 2^\circ$ thickness). Differences between the modeled and the observed paths in extended arm movements were small.

The findings in the extended arm pointing and short amplitude radial reaching movements strongly suggested that a two-dimensional Listing's surface could be implemented as a general working assumption. Nevertheless, our model based on a Listing's law constraint did not always precisely predict the experimental hand paths even in such movements. Small discrepancies between the simulated and observed paths could be attributed to reasons other than deviations from the planar assumption. In the next paragraphs, we will discuss possible sources of error in our modeling approach that might have contributed to the differences between the predicted and observed paths.

Effects of violations of the single-axis rotation assumption on the discrepancies between predicted and observed hand paths

In our model, we have adopted a flat Listing's constraint as a first-order approximation for the rotations of the upper arm. This was a simplifying assumption for assessing the success of our kinematic model in accounting for at least part of the shoulder joint behavior. Twisted manifolds were found during frontal plane movements, which could explain the discrepancies between the modeled and observed paths. However, during extended arm and radial movements of small amplitude, a flat Listing's plane was a reasonable assumption, and yet, in these conditions there were trials that did not show a full correspondence between the modeled and the observed hand paths. Such differences could be attributed to deviations from the assumption that the rotation vectors within a Listing's plane follow a straight line.

Our experimental data showed that the single-axis rotation assumption was violated throughout the movements, regardless of how close the rotation vectors of the upper arm fitted a flat Listing's plane. In a comparable experiment, Gielen et al. (1997) also reported a lack of support for fixed-axis angular velocities. This implies that rotation vectors in a Listing's plane may follow paths other than straight. A theoretical account for the possibility that a Listing's plane assumption may be independent from the direction of the axes of rotation is provided in the Appendix. This could explain the discrepancies between the simulated and observed hand paths in conditions when the rotation vectors of the upper arm closely fitted a flat Listing's plane.

Distortions in sensorimotor mapping and deviations from Listing's law

Differences between our model predictions and the experimental observations could also be caused by inaccuracies in the sensorimotor transformations that underlie reaching for visual objects in space.

Henriques and Crawford (2000) demonstrated that errors in mapping visual sensory information have a detrimental effect on the motor commands during the performance of pointing movements towards visually memorized targets situated either along vertical meridians or within the horizontal plane. For the horizontal plane movements, Henriques and colleagues (2003) provided further evidence suggesting that the transformations from (binocular) visual coordinates to spatial hand coordinates are inaccurate when the gaze is on target. They suggested that the accuracy in positioning the hand depends on the target depth relative to the eyes and relative to other target locations (Henriques et al. 2003), and is not dependent on the amplitude of the movement. In our experiments, differences between short vs long radial movements could thus be explained by the errors in mapping eye-position information and not necessarily to the incorrect implementation of Listing's law during motor execution.

Van Beers et al (2002) linked the two perceptual modalities relevant for the present study (i.e., vision or proprioception) and hand movement directions in three-dimensions. Their findings suggest that vision is dominant when changes in target position take place along the frontal plane (as in our frontal plane movements). On the other hand, proprioception becomes dominant when changes in target position require the hand to move at different depths in the orthogonal direction relative to the frontal plane of the trunk (as in our radial movements).

According to the above findings, reaching for visual targets at different radial depths leads to errors in performance that are related to sensorimotor mapping errors. Intrinsic joint control based on Listing's law may thus be more relevant during reaching at different depths in the radial direction. On the other hand, control of hand reaching based on eye-position information may be more relevant during frontal plane movements because all visual targets in this condition lie within a plane that is located at a constant depth from the eyes.

Effect of dynamics of the arm at execution on the predicted hand paths

Admiraal et al. (2001) reported that arm velocity alone may influence the fit to a Listing's surface suggesting that dynamics could affect the expression of an intrinsic kinematic plan based on a Listing's law-like strategy. The effects of interaction torques (Hollerbach and Flash 1982) during the execution of arm movements should be

mentioned at this point. Inertial, Coriolis and centrifugal forces interact in rotating arm joints during reaching for visual targets (Hollerbach and Flash 1982). Their interaction depends on the type of movement and the joint angular velocities. In the absence of an adequate cancellation or compensation for such effects, movements would deviate from the pre-planned path during their execution (Hollerbach and Flash 1982).

A possibility that should be considered for selecting a desired arm configuration and/or hand path is a strategy that involves the optimization of an objective function that is neither purely kinematic nor purely dynamic. Soechting and Flanders (1998) have examined several optimization criteria during movements in the parasagittal planes. They first reported a model based on the minimization of the rate of change of joint torques that failed to predict realistic paths, and proposed an alternative model based on the minimization of the rate of change of muscle forces that corresponded more closely with the observed hand paths. Soechting and Flanders (1998) also suggested that minimization of the peak value of the kinetic energy could account for the observed arm orientation.

The forward modeling approach presented here does not consider movement dynamics or static effects, and is purely kinematic based only on geometric constraints. The model is relatively simpler than the models proposed by Soechting and Flanders (1998). Such a simplification may pose a limitation on our model but in light of the generally successful fit between the simulated and experimental paths in extended arm and radial movements, the underlying kinematic plan appears to account for the path characteristics of some movement types. This is consistent with the results of a recent study by Hermens and Gielen (2004) that compared models based on Listing's law to other models (e.g., based on the minimization of work, torque change, or variance). In that study, it was demonstrated that the intrinsic kinematic approach based on Listing's law provides the smallest discrepancies between the measured and predicted arm postures at the end of a movement.

To conclude, the results from our model suggest the possibility that kinematic considerations do play a dominant role in the planning of joint rotations and hand paths during three-dimensional arm movements as well as in the planning of a proper orientation of the arm. A weakness of the present approach is that the model did not take into consideration the effects of dynamics, which could influence the hand trajectories at the execution stage.

Summary

Listing's law may be a valid constraint for the control of the upper arm segment at the intrinsic level in some movement conditions. We have used a modeling approach that assumed that the shoulder joint rotations

are constrained by a flat Listing's plane and single-axis rotations. We have also assumed that there is a linear relationship between the elbow and the shoulder rotations.

Support for the validity of the Listing's plane assumption was presented in the first manuscript (Liebermann et al. 2005). In this second manuscript, we show that there is no evidence for single-axis rotations. We consolidate these results by suggesting that the arm rotation vectors could lie in a Listing's plane even though they could follow paths other than straight lines within the plane.

We have shown that it is possible to account for the general kinematic characteristics of end-point paths during three-dimensional movements based on the implementation of the flat Listing's plane constraint. Our model predicted reasonably well the hand paths during pointing with an extended arm towards most directions and during short amplitude radial reaching movements. Minor discrepancies between the model and the observed paths could be explained by a violation of the single-axis rotation assumption. For movements performed in a frontal plane, the rotation vectors did not fit a Listing's plane and the differences between simulated and experimental paths were large. Static and dynamic characteristics of the arm rather than kinematics may become dominant factors in the choice of a strategy for the control of the arm orientation in frontal plane movements. Perceptual considerations may also play an important role in this case.

Future research should consider a model that includes other manifolds for Listing's law (e.g., a curved plane), and a model that predicts the extrinsic hand kinematics from constraining the rotation vectors of the upper arm to follow specific paths such as curved paths within a Listing's plane.

Acknowledgements The authors wish to thank Jason Friedman for his comments on an earlier version of this manuscript. This research was supported in part by a research grant from the Israeli Ministry of Science and by the Moross laboratory. Tamar Flash is an incumbent of the Hymie Moross Professorial chair.

Appendix

On the relationship between the path in rotation vector space and the angular velocity vector

Given the rotation vector $\vec{r}(t)$, the angular velocity can be derived according to (Hepp 1990):

$$\vec{\omega}(t) = 2 \frac{\dot{\vec{r}} + \vec{r} \times \dot{\vec{r}}}{1 + \vec{r}^2}, \quad (15)$$

where the dot denotes derivation with respect to time.

We assume that the initial and final arm configuration described by \vec{r}_a and \vec{r}_b , respectively, lie in Listing's plane.

We first show that if these rotation vectors follow a straight path in Listing's plane between the initial and final configuration, the axis of rotation is fixed in space. A straight line in rotation vector space is given by:

$$\vec{r}(\lambda) = \vec{r}_a + \lambda(\vec{r}_b - \vec{r}_a), \quad (16)$$

where λ is an arbitrary path parameter between 0 and 1.

If \vec{n} denotes the normal vector of Listing's plane, all points within Listing's plane can be described by:

$$(\vec{r} - \vec{r}_a) \cdot \vec{n} = 0. \quad (17)$$

It follows that the rotation vectors defined in (17) lie in Listing's plane since

$$(\vec{r}(\lambda) - \vec{r}_a) \cdot \vec{n} = \lambda(\vec{r}_b - \vec{r}_a) \cdot \vec{n} = 0. \quad (18)$$

The angular velocity corresponding to a straight line in rotation vector space can be obtained by inserting (16) into (15):

$$\begin{aligned} \vec{\omega}(t) &= 2 \frac{\dot{\vec{r}} + \vec{r} \times \dot{\vec{r}}}{1 + \vec{r}^2} = 2 \frac{\vec{r}' + \vec{r} \times \vec{r}'}{1 + \vec{r}^2} \dot{\lambda}(t), \\ &= 2 \dot{\lambda}(t) \frac{(\vec{r}_b - \vec{r}_a) + \vec{r}_a \times \vec{r}_b}{1 + \vec{r}_a^2 + 2\lambda(t)\vec{r}_a(\vec{r}_b - \vec{r}_a) + \lambda^2(t)(\vec{r}_b - \vec{r}_a)^2}, \end{aligned} \quad (19)$$

where the prime denotes derivation with respect to λ . Equation 20 can be written in the form:

$$\vec{\omega}(t) = \omega(t)\vec{n}_{ab}, \quad (20)$$

where

$$\omega(t) = 2 \dot{\lambda}(t) \frac{|(\vec{r}_b - \vec{r}_a) + \vec{r}_a \times \vec{r}_b|}{1 + \vec{r}_a^2 + 2\lambda(t)\vec{r}_a(\vec{r}_b - \vec{r}_a) + \lambda^2(t)(\vec{r}_b - \vec{r}_a)^2}, \quad (21)$$

$$\vec{n}_{ab} = \frac{(\vec{r}_b + \vec{r}_a) + \vec{r}_a \times \vec{r}_b}{|(\vec{r}_b - \vec{r}_a) + \vec{r}_a \times \vec{r}_b|} \equiv \text{const.} \quad (22)$$

We conclude that the angular velocity vector $\vec{\omega}(t)$ does not change its direction. It only changes its absolute value. Straight paths in rotation vector space, therefore, correspond to single-axis rotations.

We investigate next the change of angular velocity for a curved path in Listing's plane between the initial and final configuration, \vec{r}_a and \vec{r}_b . As an example, we consider a curved path in rotation vector space of the following form:

$$\vec{r}(\lambda) = \vec{r}_a + \lambda(\vec{r}_b - \vec{r}_a) + \lambda(1 - \lambda)(\vec{n} \times (\vec{r}_b - \vec{r}_a)), \quad (23)$$

where \vec{n} denotes again the normal of Listing's plane.

It should be noted that as for the straight path in Listing's plane $\vec{r}(0) = \vec{r}_a$, $\vec{r}(1) = \vec{r}_b$ and all rotation vectors (23) lie in the plane, since

$$\begin{aligned} (\vec{r}(\lambda) - \vec{r}_a) \cdot \vec{n} &= [\lambda(\vec{r}_b - \vec{r}_a) + \lambda(1 - \lambda)(\vec{n} \times (\vec{r}_b - \vec{r}_a))] \cdot \vec{n} \\ &= 0. \end{aligned} \quad (24)$$

The angular velocity follows from (15) and (23). After some algebraic transformations, we get:

$$\vec{\omega}(t) = \frac{2\dot{\lambda}(t)}{1 + [\vec{r}_a + \lambda(t)(\vec{r}_b - \vec{r}_a) + \lambda(t)(1 - \lambda(t))(\vec{n} \times (\vec{r}_b - \vec{r}_a))]^2} \cdot [(\vec{r}_b - \vec{r}_a) + \vec{r}_a \times (\vec{r}_b - \vec{r}_a) + (1 - 2\lambda(t))[\vec{n} \times (\vec{r}_b - \vec{r}_a) + \vec{r}_a \times (\vec{n} \times (\vec{r}_b - \vec{r}_a))] - \lambda^2(t)(\vec{r}_b - \vec{r}_a) \times (\vec{n} \times (\vec{r}_b - \vec{r}_a))], \quad (25)$$

which can be written, as before, in the form:

$$\vec{\omega}(t) = \vec{\omega}(t)\vec{n}_{ab}(t). \quad (26)$$

In contrast to (20), the axis of rotation in (26) is not fixed in space, but is a function of the path parameter λ . Each point of the path in rotation vector space therefore corresponds to a different axis of rotation.

References

- Abend W, Bizzi E, Morasso P (1982) Human arm trajectory formation. *Brain* 105:331–348
- Admiraal MA, Medendorp WP, Gielen CCAM (2001) Three-dimensional head and upper arm orientations during kinematically redundant movements and at rest. *Exp Brain Res* 142:181–192
- Atkeson CG, Hollerbach JT (1984) Kinematic features of unrestrained arm movements (Technical Report 790). Artificial Intelligence Laboratory, MIT, Boston, MA
- Biess A, Flash T, Liebermann DG (2001) Multijoint point-to-point arm movements of humans in 3d-space—minimum kinetic energy paths. In: Meulenbroek R, Steenberger B (eds) Proceedings of the Tenth Biennial Conference of the International Graphonomics Society. Institute for Cognition and Information Pub, Nijmegen, pp 142–147
- Ceylan M, Henriques DYP, Tweed DB, Crawford JD (2000) Task-dependent constraints in motor control: pinhole goggles make the head move like an eye. *J Neurosci* 20:2719–2730
- Collewyn H, Ferman L, Van den Berg AV (1988) The behavior of human gaze in three-dimensions. In: Cohen B, Henn V (eds) Representation of three-dimensional space in the vestibular oculomotor and visual systems. *Ann N Y Acad Sci* 545:105–127
- Craig JJ (1989) Introduction to robotics. Mechanics and control. Addison-Wesley, Reading, MA, pp 28–59
- Crawford JD, Vilis T (1995) How do motor systems deal with the problems of controlling three-dimensional rotations? *J Mot Behav* 27:89–99
- Flanagan JR, Ostry DJ (1989) Trajectories of human multijoint arm movements: evidence of joint level planning. In: Hayward V, Khatib O (eds) Lecture notes in control and information sciences. Experimental robotics I, vol 139. Springer, Berlin Heidelberg New York, pp 594–613
- Flash T, Hogan N (1985) The coordination of arm movements: an experimentally confirmed mathematical model. *J Neurosci* 7:1688–1703
- Georgopoulos AP, Lurito JT, Petrides M, Schwartz AB, Massey JT (1989) Mental rotation of the neuronal population vector. *Science* 243:234–236
- Gielen CCAM, Vrijenhoek EJ, Flash T, Neggers SFW (1997) Arm position constraints during pointing and reaching in 3D. *J Neurophysiol* 78:1179–1196
- Haslwanter T (1995) Mathematics of 3-dimensional eye rotations. *Vision Res* 35:1727–1739
- Henriques DYP, Crawford JD (2000) Direction-dependent distortions of retinocentric space in the visuomotor transformation for pointing. *Exp Brain Res* 132:179–194
- Henriques DYP, Medendorp WP, Gielen CCAM, Crawford JD (2003) Geometric computations underlying eye-hand coordination: orientation of the two eyes and the head. *Exp Brain Res* 152:70–78
- Hepp K (1990) On Listing's law. *Commun Math Phys* 132:285–292
- Hermens F, Gielen CCAM (2004) Posture-based or trajectory-based movement planning? A comparison of direct and indirect pointing movements. *Exp Brain Res* 159:340–348
- Hollerbach JM, Atkeson CG (1986) Characterization of joint-interpolated arm movements. In: Heuer H, Fromm C (eds) Generation and modulation of action patterns. *Exp Brain Res Suppl*(15):41–54. Springer, Berlin Heidelberg New York
- Hollerbach JM, Atkeson CG (1987) Deducing planning variables from experimental arm trajectories: pitfalls and possibilities. *Biol Cybern* 56:279–292
- Hollerbach JM, Flash T (1982) Dynamic interactions between limb segments during planar arm movement. *Biol Cybern* 44:67–77
- Hore J, Watts S, Vilis T (1992) Constraints on arm position when pointing in three dimensions: Donders' law and the Fick gimbal strategy. *J Neurophysiol* 68:374–383
- Hore J, Watts S, Tweed D (1994) Arm position constraints when throwing in three dimensions. *J Neurophysiol* 72:1171–1180
- Humphrey DR (1979) On the organization of visually directed reaching: contributions by nonprecentral motor areas. In: Talbot RE, Humphrey DR (eds) Posture and movement. Raven Press, New York, NY, pp 51–112
- Jeannerod M (1988) The neural and behavioral organization of goal-directed movements. Oxford University Press, Oxford
- Jeannerod M (1990) The representation of the goal of an action and its role in the control goal-directed movements. In: Schwartz EL (ed) Computational neuroscience. MIT Press, Cambridge, MA, pp 352–368
- Kaminski T, Gentile AM (1986) Joint control strategies and hand trajectories in multijoint pointing movements. *J Mot Behav* 18:261–278
- Lee D, Port NL, Georgopoulos AP (1997) Manual interception of moving targets II. On-line control of overlapping submovements. *Exp Brain Res* 116:421–433
- Marotta JJ, Medendorp WP, Crawford JD (2003) Kinematic rules for upper and lower arm contributions to grasp orientation. *J Neurophysiol* 90:3816–3827
- Medendorp WP, Crawford JD, Henriques DYP, Van Gisbergen JAM, Gielen CCAM (2000) Kinematic strategies for upper arm-forearm coordination in three dimensions. *J Neurophysiol* 84:2302–2816
- Miller LE, Theeuwes M, Gielen CCAM (1992) The control of arm pointing movements in three dimensions. *Exp Brain Res* 90:415–426
- Morasso P (1981) Spatial control of arm movements. *Exp Brain Res* 42:223–227
- Nakano E, Imamuzu H, Osu R, Uno R, Gomi H, Yoshioka T, Kawato M (1999) Quantitative examinations of internal representations for arm trajectory planning: minimum commanded torque change model. *J Neurophysiol* 81:2140–2155
- Nelson WL (1983) Physical principles for economies of skilled movements. *Biol Cybern* 46:135–147
- Richardson MJE, Flash T (2002) Comparing smooth arm movements with the two-thirds power law and the related segmented-control hypothesis. *J Neurosci* 22:8201–8211
- Schaal S, Sternad D (2001) Origins and violations of the 2/3 power law in rhythmic three-dimensional arm movements. *Exp Brain Res* 136:60–72
- Soechting JF, Flanders M (1998) Movement planning: kinematics, dynamics, or both? In: Harris L, Jenkin M (eds) Vision and action. Cambridge University Press, New York, NY, pp 332–349
- Soechting JF, Lacquaniti F (1981) Invariant characteristics of a pointing movement in man. *J Neurosci* 1:710–720

- Soechting JF, Terzuolo CA (1988) Sensorimotor transformations underlying the organization of arm movements in three-dimensional space. *Can J Physiol Pharmacol* 66:502–507
- Soechting JF, Buneo CA, Herrmann U, Flanders M (1995) Moving effortlessly on three dimensions: does Donders' Law apply to arm movements? *J Neurosci* 15:6271–6280
- Straumann D, Haslwanter T, Hepp-Reymond MC, Hepp K (1991) Listing's law for the eye, head and arm movements and their synergistic control. *Exp Brain Res* 86:209–215
- Todorov E, Jordan MI (1998) Smoothness maximization along a predefined path accurately predicts speed profiles of complex arm movements. *J Neurophysiol* 80:696–714
- Torres EB, Zipser D (2002) Reaching to grasp with a multi-jointed arm. I. Computational model. *J Neurophysiol* 88:2355–2367
- Tweed D, Vilis T (1987) Implications of rotational kinematics for the oculomotor systems in three dimensions. *J Neurophysiol* 58:832–849
- Tweed D, Vilis T (1990) Geometric relations of eye position and velocity vectors during saccades. *Vision Res* 30:111–127
- Uno Y, Kawato M, Suzuki R (1989) Formation and control of optimal trajectory in human multijoint arm movement. Minimum torque-change model. *Biol Cybern* 61:89–101
- Van Beers RJ, Wolpert DM, Haggard P (2002) When feeling is more important than seeing in sensorimotor adaptation. *Curr Biol* 12:834–837
- Vilis T, Tweed D (1991) What can rotational kinematics tell us about the neural control of eye movements? In: Humphrey DR, Freund H-J (eds) *Motor control: concepts and issues*. Wiley, New York, NY
- Viviani P, Flash F (1995) Minimum-jerk, two-thirds power law, and isochrony: converging approaches to movement planning. *J Exp Psychol Hum Percept Perform* 17:32–53
- Viviani P, Terzuolo C (1982) Trajectory determines movement dynamics. *J Neurosci* 7:431–437
- Wang X (1998) Three-dimensional kinematic analysis of influence of hand orientation and joint limits on the control of arm postures and movements. *Biol Cybern* 80:449–463
- Wang X, Verriest JP (1998) A geometric algorithm to predict the arm reach posture for computer-aided ergonomic evaluation. *J Vis Comput Anim* 9:33–47
- Westheimer G (1957) Kinematics of the eye. *J Optic Soc Am* 47:967–974
- Wolpert DM, Ghahramani Z, Jordan MI (1995) Are arm trajectories planned in kinematic or dynamic coordinates? An adaptation study. *Exp Brain Res* 103:460–470